行政院國家科學委員會專題研究計畫　期中進度報告

光學用自身組織塊式高分子/量子點奈米複合材料(1/3)

計畫類別：整合型計畫
計畫編號：NSC91-2120-M-009-001-
執行期間：91 年 08 月 01 日至 92 年 12 月 31 日
執行單位：國立交通大學材料科學與工程學系

計畫主持人：韋光華
共同主持人：林宏洲，黃中垚，陳登銘
計畫參與人員：梁耕三

報告類型：完整報告
報告附件：出席國際會議研究心得報告及發表論文
處理方式：本計畫涉及專利或其他智慧財產權，1 年後可公開查詢

中　華　民　國 92 年 9 月 29 日

Self-assembly of Block Copolymer/Quantum Dots Nanocomposites for Optical Applications

Prof. Kung-Hwa Wei (韋光華)* , Hong-Cheu Lin (林宏洲) ,
Teng-Ming Chen (陳登銘) and Jung-Y. Huang (黃中垚)

Dept. of Materials Science & Eng.
Dept. of Applied Chemistry
Institute of Eletro-optics
National Chiao Tung University

ABSTRACT

This project involves the synthesis of II-VI colloidal semiconductor nanocrystals or quantum dots (QDs) and nanostructured rod-coil block copolymers, selective distributions of QDs by hydrophilic or hydrophobic surfactants and a building of prototype photonic device. Based upon different disciplines, this project is divided into four parts. Each part is carried out by one group of professors and graduate students. The first part is concerned with a synthesis of liquid crystalline diblock copolymer containing fluorene, thiophene and biphenyl units. The second part involves a syntheses and optical characterization of II-VI group quantum dots and their core-shell structures. The third part consists of selective distributions of QD in polystyrene-b-poly(ethylene oxide) and polystyrene-b-poly(methyl methacrylate) blockcopolymer. The fourth part address nanotemplate fabricated from block copolymer thin films.

Part 1. Synthesis and characterization of self-assembled block-copolymers into nanostructures

Abstract

A series of conjugated aromatic molecules containing fluorene, thiophene, and biphenyl groups were synthesized successfully via Suzuki coupling reaction. Three alkoxyl groups with different lengthes ($-OC_8H_{17}$, $-OC_{12}H_{25}$, and $-OC_{16}H_{33}$) are connected to the conjugated cores to generate various luminescent compounds. Polyethylene oxide (PEO, Mn=750) is also used as a flexible chain to form rod-coil block molecules. Besides, similar polymeric derivatives containing conjugated fluorene units, which possess novel electro-optical and supramolecular properties, are synthesized. The direct Heck polymerization of the diphenylene vinylene-connected polyethylene oxide (PEO, Mn=1000) monomer with aromatic diiodo compound yields the polymer containing π-conjugated blocks and flexible PEO blocks.

1.1 Introduction

In recent years, the study of the organic light-emitting diodes (OLEDs) and liquid crystalline materials are widely surveyed. Generally, a liquid crystalline molecule has a rigid core and a flexible chain. For an organic light-emitting material, a conjugated rigid core is a necessary segment. Therefore, in order to combine liquid crystalline properties with organic light-emitting properties, alkoxyl groups with different lengthes are chosen as the flexible chains, and the rigid cores are designed as an aromatic conjugated rings containing fluorene, thiophene, and biphenyl groups. The development of self-assembled materials has received a great attention due to their potential in the construction of well-defined supramolecular nanostructures. Rod-coil systems[1] consisting of rigid-rod and flexible-coil segments are excellent candidates for creating well-defined supramolecular structures through a process of spontaneous organization. Thus, the rod-coil block molecules containing polyethylene oxide (PEO) as the coil-segment[2,3] and the previous conjugated rings as the rod-segment are reported.

1.2 Experimental Section

The Suzuki coupling reaction is used to synthesize one of the rigid cores. The first step of Suzuki coupling reaction is oxidative addition between catalyst $Pd(PPh_3)_4$ and one aromatic halide. Next step followed is transmetallation between Pd(II) and the other aromatic boronic acid. Finally, the two different aromatic groups react via reductive elimination to form the coupling structures. The synthetic route is shown in Scheme 1.[4,5]

Scheme 2 outlines another synthetic route for the polymer containing conjugated fluorine chromophores. The nucleophilic substitution reaction of (**7)** with PEO (**8)** in EtOH/K_2CO_3 solution yielded monomer (**9),** which produced the desired polymer (**11)** under Heck polymerization with compound (**10)**. The thermal properties, phase behavior and photoluminescence of these synthesized compounds were studied by the polarizing optical microscopy and DSC (Perkin Elmer Pyris 7).

1.3 Results and Discussion

The thermal properties and phase behavior of these compounds are presented in Table 1. Compound **FTBPOC$_8$ (2)** with a shorter alkoxyl length (R=C_8H_{17}) exhibits only the nematic phase. As usual, compounds **FTBPOC$_{12}$ (3)** and **FTBPOC$_{16}$ (4)** with longer alkoxyl lengthes (R=$C_{12}H_{25}$ and $C_{16}H_{33}$) show not only the nematic phase but also the SmA and the SmC phases. Compound **FTBPOHPEO$_{750}$ (5)** with one side of PEO exhibits the nematic phase. However, compound **FTBPPEO$_{750}$ (6)** with PEO on both sides does not possess any LC phase.

Comparing these two systems with and without PEO flexible segments, compounds with PEO have lower isotropic temperatures and PEO reduces the thermal stability of the LC phase. Nevertheless, the nematic phase in compound **FTBPOHPEO$_{750}$ (5)** with one side of PEO is still sustained at lower temperatures. The UV-Visible spectra and photoluminescent spectra are summarized in Table 2. Regardless of the different flexible chain lengths, the photoluminescent properties (solution and film) and UV-Vis spectra of the highest peaks are all similar, which is due to the same conjugated core. In solution, all of these compounds exhibit the maximum absorption peaks in the range of 400-403 nm, and the polymer **(11)** exhibit the maximum absorption peaks at 326 and 378 nm, respectively. The maximum emission peaks of the synthesized molecules and polymer **(11)** are about 446 nm and 443 nm. In solid films, the maximum emission peaks are in the range of 497-503 nm, and the polymer **(11)** shows the maximum emission peaks at 465 and 492 nm, respectively.

Scheme 1

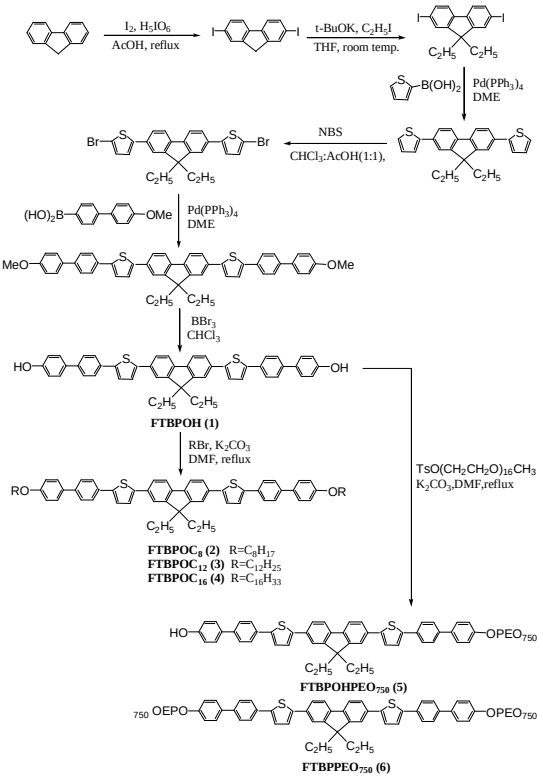

Scheme 2

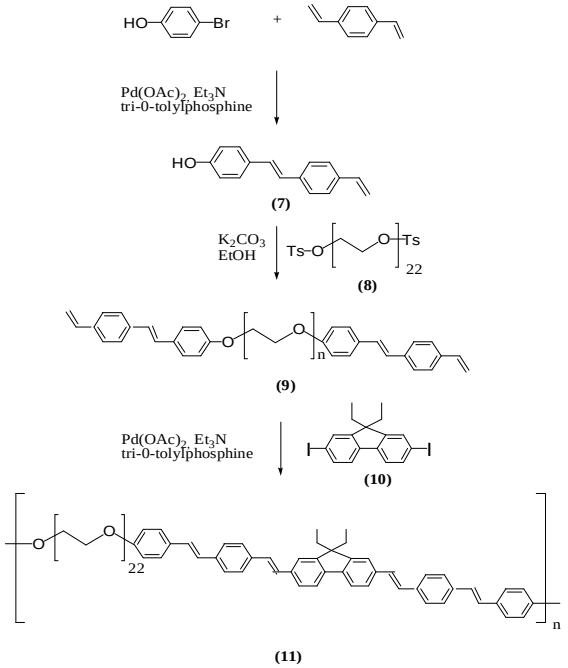

Table 1. The thermal properties and phase behavior of the synthesized molecules

Compound	**Phase Behavior (J/g)**	
FTBPOC$_8$ (2)	**K** 194.2(18.4) **N** 335.0(0.7) **I** **I** 334.0(-0.6) **N** 158.1 (-23.8) **K**	**H**$^{\#}$ **C**$^{\#}$
FTBPOC$_{12}$ (3)	**K** 163.3(11.4) **S$_A$** 248.2(0.3) **N** 283.7(0.7) **I** **I** 280.9(-0.7) **N** 245.6(-0.3) **S$_A$** 135.0(-11.0) **K**	**H** **C**
FTBPOC$_{16}$ (4)	**K** 144.7(7.7) **S$_A$** 247.7(0.3) **N** 299.1(0.1) **I** **I** 292.0**N**246.8(-0.3) **S$_A$** 199.7(-0.1)**S$_c$** 143.7(-0.1)**K'**131.7(-6.7)**K**	**H** **C**
FTBPOHPEO$_{750}$ (5)	**K** 98.8(2.7) **N** 124.7(0.06) **I** **I** 123.7(-0.08) **N** 71.5(-2.2) **I**	**H** **C**
FTBPPEO$_{750}$ (6)	*** K** 83 **I** **I** 75 **K**	**H** **C**

*：observed by polarizing optical microscope.(POM)

#：H: heating cycle. C: cooling cycle

Table 2. UV-Visible and photoluminescent properties of the synthesized molecules

Sample	**UV** $^{\#}$ **(nm)**	**PL*** **(nm) solution**	**PL*** **(nm) film**
(1)	**403**	**446,474**	**498,531**
(2)	**402**	**447,475**	**500,526**
(3)	**402**	**446,474**	**498,533**
(4)	**403**	**446.462**	**497,529**
(5)	**400**	**447,472**	**503,529**
(6)	**402**	**446,474**	**503,528**
(11)	**326,378**	**443,464**	**465,492**

#： dissolved in THF.

*：excited wavelength is 400nm

Part 2A. Synthesis and Optical Characterization of Ⅱ-Ⅵ Group Semiconductor

Nanocrystal (Quantum Dots)

Abstract

The synthesis, optical and structure properties of Ⅱ-Ⅵ group semiconductor nanocrystal (quantum dots) are investigated. To comprehend optical and structure properties through UV-Vis absorbance spectra, photoluminescence spectra, X-ray diffraction spectra, TEM pictures.

2A.1. Introduction

Colloidal semiconductor nanocrystals have generated great fundamental and technical interest in recent years.[6-8] The size-dependent emission is probably the most attractive property of semiconductor nanocrystals. Due to quantum size effects,[8] the band gap of CdSe nanocrystals increases as their size decreases, and thus the emission color of the band-edge PL of the nanocrystals shifts continuously from red (centered at 650nm) to blue (centered at 450nm) as the size of the nanocrystals decreases. Since Murray et al.[9] reported the synthesis of high quality CdSe nanocrystals using dimethyl cadmium ($Cd(CH_3)_2$) as the cadmium precursor, the synthesis of CdSe nanocrystals using this precursor has been well developed.[10-12] ($Cd(CH_3)_2$) is extremely toxic, pyrophoric, expensive, unstable at room temperature, and explosive at elevated temperatures by releasing large amount of gas. Due to this reasons, the ($Cd(CH_3)_2$)-related schemes require very restricted equipments and conditions. So we use CdO replace ($Cd(CH_3)_2$) to synthesis CdSe. This new synthetic scheme works significantly better than the ($Cd(CH_3)_2$)-related ones.

2A.2. Results and Discussion

The temporal evolution of CdSe nanocrystals have quantum-size effect in the UV-vis and PL spectra, shown in Figure 1. With the increasing of reaction time, the particle size increases, peak shifts to long wavelength. This is red-shift phenomenon. There are 20 ~ 30 Stokes' shift between absorbance and photoluminescence wavelengths.

CdSe exhibit a wurtzite crystal structure with the lattice spacing of the bulk materials. The wurtzite structure belongs to hexagonal close packing. Figure 2. shows the XRD pattern of four different reaction time of CdSe. The position of reflections for wurtzite structure CdSe are indicated. CdSe with short reaction time has peaks between 30 ~ 40 degrees and 55 degrees. We find that it is CdO peak, means the precursor react incompletely. So we need to improve the synthesis condition.

Part 2B. Synthesis and Characterizations of II-IV Semiconductor Quantum Dots for Photonic Nanopcomposites

Abstract

This research is attempted to investigate the synthetic methodology and luminescent properties of group II-VI quantum dots (QDs). The report describes the preparation, microstructure, UV-VIS and photoluminescence spectra of two series of core-shell type CdSe/MS (M = Cd, Zn) QDs.

2B.1. Introduction

Colloid semiconductor nanoparticles or quantum dots (QDs) have received much attention in recent years. Quantum confinement effect has been observed in various semiconductor QDs of CdSe or core-shell type CdS/MS/MS (M = Cd, Zn) derived from a simple chemical colloidal method.

Other than the synthesis and characterization of QDs, we will also investigate the possibility of integration of pristine or core-shell QDs into a solid-state matrix of block copolymer by appropriate surface modification with hydrophilic or hydrophobic functional groups.

2B.2. Results and Discussion

The TEM images for the green-emitting CdSe/ZnS QD are represented in Fig. 2, respectively. The spherical dots with diameter of 2 nm were identified as CdSe/ZnS QDs. We have observed decent dispersion of the QDs and no stacking or agglomeration was observed, as indicated in the single-layer structure in Fig. 1. The well-dispersed QDs with single layer structure can be easily formed with effective control of the QD concentration in the solution. With effective control of the synthetic conditions, we have successfully synthesized different types of core-shell CdSe/MS (M = Cd, Zn) QDs. We have also compared and investigated the effect of shell materials on the luminescent properties of CdSe/MS QDs and the results are represented in the PL spectra shown in Fig. 2. We have discovered that the pristine and uncoated CdSe QDs exhibit the weakest luminescence, whereas the luminescence intensity of CdSe/ZnS was found to be twice as strong as that of CdSe/CdS. As a shell material with a larger band gap, ZnS (E_g = 3.68 eV) was empirically found to exhibit stronger quantum confinement than CdS (E_g = 2.42 eV), as indicated in the PL spectra shown in Fig. 2.[13] Thus, the design and exploration of new shell materials to enhance the luminescence intensity of QDs will be one of the most important future work in this research

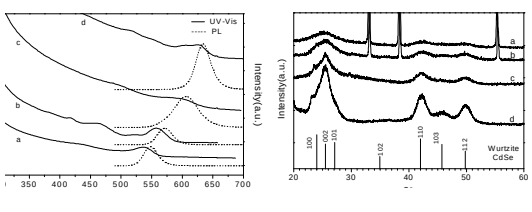

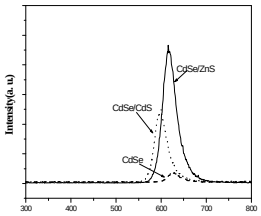

Fig. 1

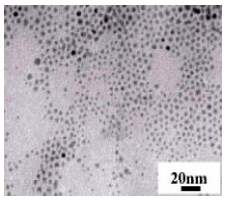

Fig. 2

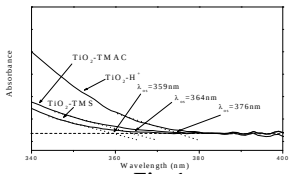

Fig. 1

Part 3. Selective Distribution of Surface-modified CdS and TiO2 Quantum Dots in PS-b-PEO and PS-b-PMMA Diblock Copolymers

Abstract

Ordered aggregates of surfactant-modified TiO_2 nanoparticles in the selective block of lamellar assemblies of the diblock copolymer PS-b-PMMA have been prepared. The hydrophobic or hydrophilic nature of the tethered surfactant determines the location of TiO_2 nanoparticles in the corresponding block. The modes of dispersion of TiO_2 in the blocks depend on the type of bonding between the surfactant and TiO_2.

Surface-modified colloid CdS quantum dots are found to selectively disperse in the poly(ethylene oxide) block of the diblock copolymer polystyrene-b-poly(ethylene oxide) (PS-b-PEO) through the interaction of the surfactant and PEO block. The incorporation of CdS quantum dots in the PEO domain results in a large reduction in PEO crystallinity and in turn induces the PEO domain to form a body-centered cubic or simple cubic structure.

3.1. Introduction

Block copolymers are versatile platform materials because they can self-assemble into various nanostructures with period thicknesses between 10 to 100 nm under the appropriate compositions and conditions, owing to microphase separation between incompatible blocks.[14-16] These block copolymer assemblies can be very useful in nanotechnology. Moreover, block copolymers can be used as nano-templates to control the spatial arrangement of nanoparticles in thin films [18] or in bulk[19] as nano-masks for lithography[20], or for photonic crystal applications.[21]

For semiconductor nanoparticles with sizes close to their Bohr exciton radius (typically between 1-10 nm), the size-dependent band gap results in tunable optical properties.[22-23] These semiconductor nanoparticles are termed as quantum dots (QDs) because their tunable optical properties can be predicted by quantum mechanics.

In this report, we report on dispersing surfactant-modified TiO_2 nanoparticles into either block of a PS-b-PMMA diblock copolymer with an ordered lamellar phase. In CdS/PS-b-PEO nanocomposites systems, the selective distribution of CdS QDs in the PEO block of a diblock copolymer, PS-b-PEO, result in morphological changes. Specifically, CdS QDs induce the PEO domains to change from hexagonally-packed cylinders to body-centered cubic or simple cubic spheres.

3.2. Results and Discussion

In TiO2/PS-b-PMMA systems, Figure 1 shows the UV-vis spectra of TiO_2-TMAC、TiO_2-H^+ and TiO_2-TMS solutions. The concentration of TiO_2 nanoparticles in both colloidal solutions is about $6\times10^{-5}\ M$. The shifts in the UV-vis absorption onset of these TiO_2 colloidal solutions suggest that the TiO_2 nanoparticles have quantum-confined properties.

Table 1 shows the calculated radii of TiO_2 particles in the colloidal solutions.

Table 1. Onset of UV-vis absorbance and calculated radii of TiO_2 nanoparticles.

	Absorbance onset wavelength (nm)	radius (nm)
TiO_2-TMAC	359	0.96
TiO_2-TMS	364	1.07

TiO_2-H^+	376	1.59

Figure 2(a) shows the lamellar morphology of PS-b-PMMA after staining with RuO_4. The periodic lamellar thickness of PS-b-PMMA is about 50 nm. The dark region is the PS domain, owing to staining, and the PS volume fraction of PS-b-PMMA is 0.55, which falls into the ordered lamellar phase region (a PS volume fraction between 0.34~0.62). The TiO_2-TMAC/PS-b-PMMA morphology is shown in Figure 2(b). In Fig. 2(b), the presence of TiO_2 in the dark spots is confirmed by EDS (Figure 2(c)), the size of TiO_2 aggregates (dark spots) is about 15-20nm. The Ti band peak indicates the existence of TiO_2 at the PS domains, while the presence of Cu peaks is caused by the Cu grid used in the sample preparation. In Figure 2(d), the gray phase is the PS domain, which is a result of staining with RuO_4, while the light phase is the PMMA domain. Dark TiO_2 nanoparticles are found to disperse in the gray domain (PS domain) in the lamellar PS-b-PMMA.

That the TiO_2-TMAC nanoparticles can be dispersed in the PS domain corresponds to the fact that both the cetyl trimethyl ammonium chloride (TMAC), containing 10 methylene units, and the polystyrene domain are hydrophobic and miscible. The presence of TiO_2-TMAC in the PS domain is further supported by differential scanning calorimetry (DSC) results. The Fourier-transform infrared (FTIR) spectra of TiO_2/PS-b-PMMA nanocomposites are shown in Figure 3. The peaks at 1741 cm^{-1}

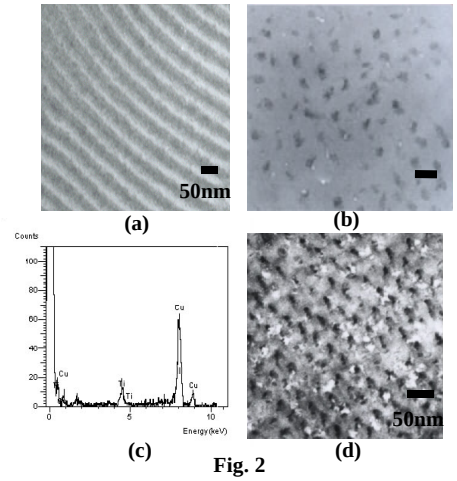

Fig. 2

and 1726 cm^{-1} result from the carbonyl groups of the PMMA domain in neat PS-b-PMMA. The carbonyl band of TiO_2-TMS/PS-b-PMMA shifts to lower wavenumbers (from 1726 to 1714 cm^{-1}) as compared to that of PS-b-PMMA. This indicates the possibility that TiO_2 is present in the PMMA domain since hydrogen bonding between the remainder of the dangling -OH groups on the surface of TiO_2 and the carbonyl groups of the PMMA domains causes the carbonyl band to shift to smaller wavenumbers.

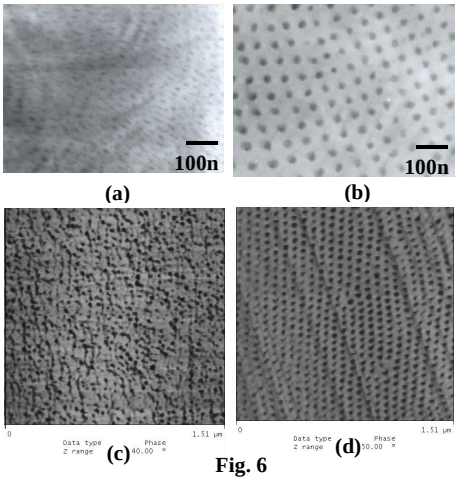

Fig. 6

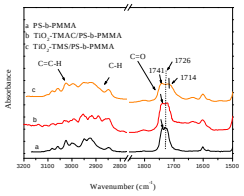

Fig. 3

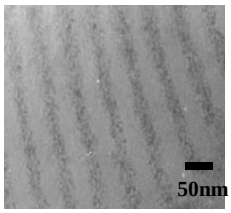

Fig. 4

Figure4 shows a transmission electron microscopy image of TiO_2-TMS/PS-b-PMMA. That the TiO_2 nanoparticles are dispersed rather uniformly in the PMMA phase is consistent with the fact that TMS contains methacrylate structures. The difference in the modes of dispersion of TiO_2 in PS and in PMMA domains can be manifested by the bonding difference between the surfactants and TiO_2. In the TiO_2-TMAC/PS-b-PMMA case, the polar-ionic bondings between TiO_2 surfaces and TMAC are weak and hence allow TiO_2 nanoparticles to rearrange to form aggregates during the solvent removal process. Whereas, in the TiO_2-TMS/PS-b-PMMA case, TMS is bonded to TiO_2 surfaces covalently, and this type of bondings is well maintained during the solvent removal process. The synthesized CdS QDs were collected and then dispersed in N, N-dimethylforamide, and their basic properties are given in Table 2.

Table 2 Characteristic Properties of CdS nanoparticles

Absorption onset (ëo)[a]	Particle size in DMF[b]	Emission wavelength[c]	Crystal size[d]	Average particle size[e]
447 nm	3.37 nm	650 nm	1.33 nm	2.5 nm

[a] The onset absorption wavelength of CdS nanoparticles in DMF as obtained from UV-vis spectra.
[b] The sizes of CdS nanoparticles in DMF were calculated with the onset absorption obtained by UV-Vis spectra using the following equation.
[c] The emission wavelength is determined from the photoluminescence.
[d] Crystal sizes are calculated using the Debye-Scherrer equation.
e The averaged size of CdS was obtained from SAXS curves of CdS/PS-b-PEO in Figure 7.

Figure 5 shows one-dimension small-angle X-ray scattering patterns (SAXS) of PS-b-PEO and CdS/PS-b-PEO nanocomposites by synchrotron radiation. For pure PS-b-PEO, four peaks appear at Q = 0.016, 0.027, 0.032 and 0.042 $Å^{-1}$, corresponding to a ratio of $1:3^{1/2}:4^{1/2}:7^{1/2}$. This ratio indicates typical scattering by hexagonally-packed cylinders (HEX). The inter-cylinder distance (D) was determined to be 45.3 nm by equation (1).

$$D = \left(4/3\right)^{1/2} * d_{100} \qquad (1)$$

Where $d_{100}=2ð/Q_{100}$ and $Q_{100}= 0.16\ nm^{-1}$. In the case of PS-b-PEO containing 0.35% CdS, the scattering peaks are located at Q = 0.0114, 0.0158, 0.0203, 0.0228, 0.0281 and 0.0399 $Å^{-1}$, which gives a ratio of 1: $2^{1/2}:3^{1/2}:4^{1/2}:6^{1/2}:12^{1/2}$. This ratio implies that the scattering is caused by either body-centered cubic packed spheres (BCC) or simple cubic spheres (SC). The inter-sphere distance is 67.5 nm, as determined from equation (2).

$$D = \left(3/2\right)^{1/2} * d_{110} \qquad (2)$$

Where $d_{110}=2ð/Q_{110}$ and $Q_{110}= 0.114\ nm^{-1}$. SAXS results confirm that the nanostructured HEX structure of pure PS-b-PEO has been transformed to a BCC or SC morphology, due to the presence of CdS QDs. The size of CdS QDs in the block copolymer is about 2.5 nm, as derived from the structure

form of the SAXS curve.

Figure 6(a) and (b) show the transmission electron microscopy (TEM) images of PS-b-PEO stained with OsO_4 and CdS/PS-b-PEO without staining, respectively. PEO domains appear in dark phase in Figure 6(a), owing to selective staining, and display as short cylinders. In the case of CdS/PS-b-PEO, however, periodic dark spherical phases of CdS-included PEO appear, and no pure PEO domains without CdS QDs could be observed. The location of CdS in the PEO domain is revealed by energy dispersive spectrometry. Dark phases are caused by the higher electron density of cadmium relative to that of PS-b-PEO. The selective distribution of mercaptoethanol-modified CdS in the PEO domain is quite possibly due to dipole-dipole interactions between the hydroxyl groups of mercaptoethanol and the PEO block. The diameter of CdS-included PEO spheres is approximately 23 nm and the inter-sphere distance is about 60 nm, as estimated from their TEM images. In order to cover all PEO domains, there must be some distributions of CdS QDs in each PEO domain because the volume fraction of added CdS with respect to the PEO block is about 2.7%, which is not enough to cover each PEO domain fully. It is, however, not possible to detect them with the current techniques. The results from TEM analysis are consistent with those by SAXS. Further evidence of the two different morphologies can be found in phase-contrast atomic force microscopy images (AFM) of PS-b-PEO and CdS/PS-b-PEO samples, as shown in Figure 6(c) and (d), respectively. A diamond knife used during the microtoming process causes the oblique lines in these figures. Figure 7(a) shows the thermal analysis results of PS-b-PEO and CdS/PS-b-PEO by differential scanning calorimetry. A crystal melting peak at 42.9°C associated with the PEO domain and a glass transition temperature (Tg) at 99 °C attributed to the PS domain appear in the pure PS-b-PEO case (the amorphous phase of PEO is rather small and undetectable). In the presence of CdS, the crystal melting peak of PEO depressed and

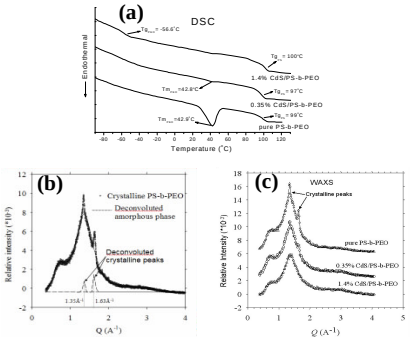

Fig. 7

diminished to a small kink, with an apparent Tg of -56.6 °C; The PS domain, however, maintains a Tg of about 99 °C. The difference between the two cases can be explained by a loss of crystallinity in the PEO domain by the infiltration of CdS QDs into the PEO domain. Moreover, the wide-angle X-ray diffraction results shown in Figure 7(b) and 7(c) also support the corresponding crystal-to-amorphous change of the PEO domain. In the case of pure PS-b-PEO, two sharp peaks at 1.35Å^{-1} and 1.63Å^{-1} represent the crystallinity peaks of the PEO domain after deconvolution, as shown in Figure 7(b). Figure 7(c) shows amorphous X-ray diffraction curves when CdS is incorporated into the PEO domain, indicating the change from crystalline to amorphous PEO. This result is also consistent with those obtained by DSC. The possible scenario for this phenomenon is due to the relatively small size of CdS to the contour length of PEO block (2.5nm vs. 130nm) and the dipole-dipole interaction between the angling hydroxy group of surface-attached mercaptoethanol on CdS and ethylene oxide in PEO domain, CdS are tethering to PEO chain and appears to destroy the crystallinity of PEO domain. This enables CdS-infiltrated PEO domains to be amorphous and to minimize their surface energy by forming either BCC or SC structures.

When only the volume fraction of the block copolymer PS-b-PEO is considered, it is true that in the equilibrium state the pure PS-b-PEO should be in the spherical region with body-center cubic packing due to strong segregation. The morphology of asymmetric amorphous-crystalline block copolymers, however, depends on both the microphase separation of the two blocks and the crystallization kinetics of the crystallizable block as demonstrated in the work by de Jeu et al.[25] In their study, lamellar or hexagonally perforated lamellar structures of PS-b-PEO were obtained even though the volume fraction of PS-b-PEO indicates that it is typically within the morphological range of sphere or cylinders. In our study, the hexagonally-packed cylindrical morphology of PS-b-PEO represents a compromise between the microphase separation involving PS and PEO blocks and the crystallization kinetics of the

PEO block. The cylindrical morphology of pure PS-b-PEO is in a meta-stable state due to the fast crystallization of the PEO block. The addition of CdS quantum dots into the diblock copolymer inhibits the crystallization of PEO block. The resultant morphology of CdS/PS-b-PEO sample, therefore, is determined largely by the microphase separation involving PS block and CdS/PEO block, (i.e. the crystallization effect is no longer existing).

3.3. Conclusions

The modes of dispersion of TiO_2 nanoparticles in different blocks are determined by the type of bondings between the surfactant and the nanoparticles. In CdS/PS-b-PEO cases, semiconductor CdS QDs can be selectively dispersed in the PEO domain of PS-b-PEO block copolymer by using a surfactant. The CdS-infiltrated PEO domains are transformed from originally hexagonally-packed cylindrical structures to BCC or SC structures because CdS inhibits the crystallization and minimizes the surface energy of CdS-infiltrated PEO phase.

Part 4. Nanotemplate from oriented block copolymer thin film

Abstract

The self-assembled, periodic structures with block copolymers with well-defined sizes and separations distances on the tens of nanometer length scale have been recognized as a promising means to functional nanostructure.[26-29] Block copolymer could self-assemble into highly ordered arrays of nanostructure to produce nanoporous template. The size and the type of ordering can be controlled by changing the molecular weight, chemical structure, molecular architecture, and composition of the block copolymers.

4.1. Introduction

Self-assemble block copolymers can be prepared for nanostructures with period thicknesses between 10 to 100 nm under the appropriate compositions and conditions, owing to microphase separation between dissimilar blocks[31]. These kind of block copolymers can be very useful in nanotechnology such as large-area periodic nanostructures can be fabricated using self-assembled block copolymers as templates.[32] Moreover, block copolymers can be used as nano-templates to control the spatial arrangement of nanoparticles in thin films as nano-masks for lithography,[31] or in photonic crystal applications.

4.2. Material and Experimental

For the present study, an asymmetric polystyrene-b-polymethylacrylate diblock copolymer (PS-b-PMMA) with a molecular weight ratio of 130.7K/46K has been used. The volume fraction of PMMA in this PS-b-PMMA is 0.70, with a polydispersity of 1.10. We produce the template for nanorods using diblock copolymers composed of polystyrene and polymethylacrylate. We dissolve the copolymer in toluene to make the dilute solution and spin on glass/ Si wafer. Subsequently, the film was annealed at 90 for 24h. Film with a thickness of 150 nm were prepared by spin coating and measured by AFM. For the morphologies observation can be found in phase-contrast atomic force microscopy images (AFM) of PS-b-PMMA after annealing for 24h (Fig. 1). For the deep UV exposure were placed the annealed sample under UV lamp to degrade the PMMA and crosslink the PS matrix such that the degrade PMMA can be removed by acetic acid rinse. We observe the morphology by SEM (Fig. 2) to make sure the template was produced.

4.3. Conclusions

The highly ordered nanotemplate can be formed by controlling the molecular weight, annealing treatment and the thickness of the thin film.

REFERENCE

(1) Lee, M.; Cho, B. K.; Zin, W. C.; *Chem. Rev.* **101**, 3869 (2001).
(2) Lee, M.; Oh, N. K.; *J. Mater. Chem.* **6**, 1079 (1996).
(3) Lee, M.; Cho, B. K.; Jang, Y. G.; Zin, W. C.; *J. Am. Chem. Soc.* **122**, 7449, (2000).
(4) Miyaura, N.; Suzuki, A.; *Chem. Rev.* **95**, 2457 (1995).
(5) Byron, D. J.; Komitov, L.; Matharu, A. S.; Wilson, R. C.; *J. Mater. Chem.* **6**, 1871 (1996).
(6) Heath, J. R.; Ed. *Acc. Chem. Res.* **1999**, Special Issue for Nanostructures, review articles relevant to colloidal nanocrystals.

(7) Alivisatos, A. P.; *Science* **271**, 933-937 (1996).
(8) Brus. L. E.; *J. Chem. Phys.* **90**, 2555 (1986).
(9) Vossmeyer, T. et al.; *J. Phys. Chem.* **98**, 7665-7673 (1994).
(10) Peng, X. G. et al.; *Nature* **404**, 59-61 (2000).
(11) Peng, Z. A. et al.; *J. Am. Chem. Soc*, **123**, 1389-1395 (2001).
(12) Peng, X. G. et al.; *J. Am. Chem. Soc.* **120**, 5343-5344 (1998).
(13) P. Reiss et al.; *Nano Lett.* **2(7)**, 781-784 (2002).
(14) Henglein, A.; *Chem. Rev.* **89**, 1861 (1989).
(15) Wang, Y et al.; *J. Phys. Chem.* **95**,525 (1991).
(16) Murry, C. B et al.; *Science* **270**, 1995.
(17) Bates, F. S. *Science* **251**, 898 (1991).
(18) Thomas, E. L. *Science* **286**, 1307 (1999).
(19) Sankaran, V. et al.; *J. Am. Chem. Soc.* **112**, 6858 (1990).
(20) Cummins, C. C. et al.; *Chem. Mater.* **4**, 27 (1992).
(21) Kane, R. S. et al.; *Chem. Mater.* **8**, 1919 (1996).
(22) Tassoni, R. et al.; *Chem. Mater.* **6**, 744 (1994).
(23) Yue, J. et al.;. *J. Am. Chem. Soc.* **115**, 4409 (1993).
(24) Li, L. et al.; *Macromolecules* **36**, 529 (2003).
(25) T. Thurn-Albrecht et al.; Adv. Mater. **12**, 787 (2000)
(26) C. T. Black et al.; Appl. Phys. Lett. **79**, 409 (2001)
(27) H. C. Kim et al.; Adv. Mater. **14**, 274 (2002)
(28) H. C. Kim et al.; Adv. Mater. **13**, 795 (2001)
(29) F. S. Bates, Science **251**, 898 (1991)
(30) S. Choi, K. M. Lee, C. D. Han, N. Sota, and T. Hashimoto, Macromolecules **36**, 793 (2003).
(31) J. Y. Cheng, C. A. Ross, E. L. Thomas, Henry I. Smith, and G. J. Vancso, Appl. Phys. Lett. **81**, 3657 (2002).

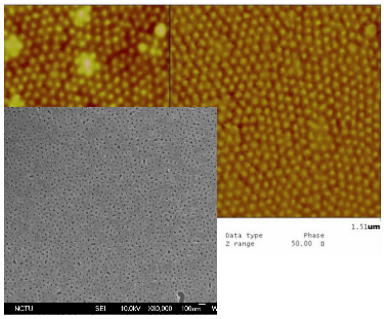

Fig. 2